Theoretical investigation of natural convection heat transfer in inclined and fully divided CO_2 enclosures on Mars

Yue Sun [a], Guiping Lin [a], Yu Jia [a,*], Dongsheng Wen [a,b], Lizhan Bai [a]

[a] Laboratory of Fundamental Science on Ergonomics and Environmental Control, School of Aeronautic Science and Engineering, Beihang University, Beijing 100191, PR China

[b] School of Chemical and Process Engineering, University of Leeds, Leeds LS2 9JT, UK

Abstract: This work presented extensive numerical studies on fluid flow and heat transfer in inclined and fully divided CO_2 enclosures with partitions on Mars. An atmospheric pressure of 1000 Pa, a gravitational acceleration of 3.62 m/s^2, and a Prandtl number of 0.77 were considered in the computation. The hot and cold walls were maintained at uniform temperatures of T_h = 240 K and T_c = 200 K, while the others were assumed as adiabatic, and the boundary condition of partitions was assumed as coupled. The velocity fields, temperature contours, and heat flux through CO_2 enclosures were presented for a Rayleigh number of 7270, an aspect ratio of 7.14, tilt angles from 0° to 90°, and partition numbers of 0, 1, 2, and 3. It was observed that three flow regimes formed successively when the tilt angle increased, namely the Rayleigh–Bénard convection, transition convection, and single-cell convection. The transition regime was the most unstable regime. The values of two critical tilt angles between the three flow regimes were also obtained. With increasing angle, the heat flux slightly decreased in the first regime, significantly decreased in the second regime, and initially increased and then slightly decreased in the third regime. The opposite effect of partitions on the first and the third regimes was explained by the field synergy principle. The partition advanced the formation of the single-cell convection to a lower angle and also alleviated the fluctuation in the heat flux for various tilt angles, which contributes to the future thermal design of Mars rovers operating on rugged Mars surface.

Keywords: carbon dioxide (CO_2) enclosure; natural convection; tilt angle; partitions; three regimes; Mars

* Corresponding author. Tel.: +86 10 82338600
E-mail address: yujia@buaa.edu.cn

1 Introduction

Enclosures are widely used in several industrial applications for heat conservation such as design of solar collectors, multilayered walls, electronic equipment cooling, and double pane windows. Furthermore, natural convection inside the vertical and horizontal enclosures is extensively examined in different operating environments. However, in addition to being influenced by the different conditions in which enclosures are located, fluid flow and heat transfer inside the enclosure also significantly differ when the inclination of the enclosure changes or when the enclosure is divided by partitions. Therefore, several studies focused on the effect of the tilt angle and partitions attached to the enclosure on heat transfer. In typical applications, air-filled cavities on the Earth were mostly reviewed as discussed below.

The investigations of heat transfer in classical enclosures are presented in several studies[1–7] and include the horizontal enclosure with heated bottom wall, cooled top wall, and two adiabatic vertical walls or the vertical enclosure with heated left wall, cooled right wall, and two adiabatic horizontal walls.

After investigating the classical cases, a few studies indicated that the diverse tilt angle of the enclosure also significantly impacted heat transfer through the enclosure. Soong et al. [8] examined natural convection and hysteresis phenomena in an air rectangular enclosure for different Rayleigh numbers ranging from 10^3 to 2×10^4 and angles from 0° to 90°. They indicated that the flow pattern was related to the initial state of the flow contours. Tzeng et al. [9] investigated the effect of the inclination on fluid flow in a two-dimensional tilted air rectangular enclosure. He pointed out that natural convection in enclosures was extremely sensitive to the inclination of the enclosure at a few critical conditions and heat transfer rate was bound with the cellular flow pattern. Girgis [10] conducted a similar study as Tzeng et al. [9]. He obtained the Nusselt number correlations. Miroshnichenko and Sheremet [11] performed an investigation of the turbulent natural convection in a square enclosure with a local heat source when the tilt angle increased from 0° to 180°. They indicated that heat transfer rate reached the maximum when the tilt angle was 150°.

Several studies focused on heat transfer and fluid flow in the enclosure with different partitions. Most of them studied partially divided enclosures and considered different locations of partition. Jetli [12] et al. performed numerical investigation of natural convection in an air square enclosure with two baffles attached to the top and bottom walls. They found that when the top baffle got closer to the cold wall and bottom baffle got closer to the hot wall, the Nusselt number decreased. Kelkar and Patankar [13] and Sun and Emery [14] proposed that the effect of the baffle on heat transfer was negligible when the height of baffle was shorter than the half of the enclosure height. Sankhavara and Shukla [15] numerically analyzed fluid flow in partially divided horizontal air rectangular enclosures with partitions attached to the vertical walls. They pointed out that the convection dominated heat transfer for higher Rayleigh numbers, while conduction dominated heat transfer for lower Rayleigh numbers. Ilis et al. [16] numerically investigated natural convection heat transfer in an air square cavity with a ceiling-mounted barrier. They found that the influence of the barrier on heat transfer decreased with increasing Rayleigh number. Yucel and Ozdem [17], Nardini et al. [18], and Bae et al. [19] indicated that heat transfer increased with increasing Rayleigh number in partially partitioned enclosures, and this was identical to that in classical cases.

A few studies focused on the fully divided enclosures. Bejan [20] numerically investigated the influence of obstructions on natural convection in two-dimensional air layers. He proposed that the horizontal adiabatic partitions increased heat transfer rate in a convection-dominated regime. Turkoglu and Yücel [21] numerically analyzed heat transfer in divided air rectangular enclosures with conducting partitions. They pointed out that the Nusselt number increased with increasing Rayleigh number, and the effect of aspect ratio on heat transfer was limited in the cases considered in the study. Kahveci [22] used polynomial differential quadrature (PDQ) method to investigate the natural convection in an air rectangular enclosure with a vertical partition. He found that a transition from the unicellular flow to multicellular flow occurred when the aspect ratio increased, and this increased the convective heat transfer coefficient. Williamson and Armfield [23] investigated fluid flow in a two-dimensional air rectangular cavity with a vertical partition placed at the middle of the cavity. They observed that when the Rayleigh number increased, an additional regime existed between the convectively unstable regime and turbulent regime unlike that in the classical cavity. Khatamifar et al. [24] numerically studied the conjugate natural convection flow in an air square cavity divided by a partition with limited thickness. They indicated that the Nusselt number increased with decreases in the partition thickness and was negligibly influenced by the partition position.

Reported studies that combine the effect of both tilt angle and partition number on heat transfer inside the enclosure are still very limited. Acharya and Tsang [25] numerically investigated the natural convection in an inclined air rectangular enclosure with a complete partition attached to the middle of the enclosure at tilt angles of 30°, 45°, 60°, and 90°. They indicated that the temperature of partition increased monotonically along its length, and the influence of Rayleigh number on the partition temperature was limited when the tilt angle was 45°. Tsang and Acharya [26] performed a numerical study on the natural convection in an inclined air rectangular enclosure with an off-center complete partition at tilt angles of 30°, 45°, 60°, and 90°. They pointed out that the effect of partition location on the partition temperature distribution decreased with increasing Rayleigh number. Mamou et al. [27] focused on the natural convective in a slanting air rectangular cavity consisting of multiple layers divided by baffles. They predicted the critical Rayleigh number for the transition from pure heat conduction to nature convection.

For the aim of exploring Mars, an increasing number of Mars rovers will work on the Mars surface in the future. Given the fact that the atmosphere on Mars surface is predominantly composed of Carbon Dioxide (CO_2) with low pressure (1000 Pa) and low temperature (200 K), thermal insulation materials and CO_2 gas enclosures are always adopted to insulate and protect the internal equipment. Hence, heat transfer characteristics of CO_2 enclosures are a key factor in the thermal design of Mars rover. Furthermore, when the Mars Rover executes the task on Mars surface covered with various sags and crests, the enclosures of the Mars Rover tilt into different angles from 0^o to 90^o. Occasionally, in order to improve the strength of the enclosure or divide the enclosure into different functional zones, full plates (the length of the plates equals to the thickness of the enclosure) are attached to the isothermal surfaces inside the enclosure. Therefore, the combined effect of the tilt angle and the partitions attached to the isothermal walls on heat transfer and fluid flow inside the enclosure should be investigated, and this can be a vital issue that influences the thermal insulation configuration and internal equipment layout of a Mars rover.

As indicated in the aforementioned review, there is a paucity of studies on the heat transfer inside the inclined and divided CO_2 enclosures on the surface of Mars. In a previous study [28], an investigation was conducted to examine the effects of enclosure aspect ratio and Grashof number on the heat transfer in classical CO_2 enclosures (non-partitioned vertical and horizontal enclosures). However, in the present study, the influence of partition number and tilt angle on the heat transfer in fully divided CO_2 enclosures on Mars surface was studied. Given the Earth surface condition, a few studies [20–27] focused on familiar issues. However, to the best of the author' knowledge, only Bejan [20] and Kahveci [22] considered the boundary conditions of the partition as the coupling, and only Bejan [20] focused on the cases in which the partitions were attached to the isothermal walls rather than the adiabatic ones. However, neither considered the effect of the partition number and enclosure angle, which was the focus of the present study. Additionally, the aspect ratios in the cases of Ar = 2, 1.5, 0.25~4, 1~2, 1, 2, 4, and 1 in Ref. [20–27], respectively, were not high as Ar = 7.14 as examined in the present study. Furthermore, no aforementioned studies offered the conception of the transition regime between the Rayleigh–Bénard regime and single-cell regime when the tilt angle increased from 0º to 90º.

This paper pays attention to numerical studies on fluid flow and heat transfer characteristics inside an inclined and fully divided CO_2 enclosure on Mars surface. The primary aspects of the study are as follows: 1) conducting numerical simulation of fluid flow and heat transfer inside an inclined and fully divided CO_2 enclosures to analyze the influence of the tilt angle and partition number on fluid flow and heat transfer mechanism; 2) obtaining the critical tilt angles that divide the evolution process of heat transfer into three successive regimes as follows: the Rayleigh–Bénard convection, transition convection, and single-cell convection; 3) achieving the heat flux through the enclosure as the function of tilt angle for different partition number, and further explaining the different function relationship features of the three flow regimes; and 4) interpreting the opposite effect of the partitions on heat transfer between the first and third regime by the field synergy principle (FSP).

2 Problem description and method

2.1 Physical model

The schematic model of an inclined enclosure filled with multiple parts separated by equally spaced finite partitions (N = 2 as an example) was shown in Fig. 1 with length L = 1000 mm, thickness H = 140 mm, and partition number N = 1, 2, 3. The tilt angle θ with respect to the horizontal plane ranged from 0° to 90°. The long sidewalls were maintained at two different temperatures T_h = 240 K and T_c = 200 K, while the short sidewalls were adiabatic. The enclosure was filled with carbon dioxide with a pressure of 1000 Pa. The enclosure depth (the length in the perpendicular direction of the xy plane) was sufficiently large (1000 mm) in comparison to the enclosure thickness (140 mm), so the effect of the adiabatic boundary condition in the perpendicular direction of the xy plane was negligible and a two-dimensional model was assumed, and this was also confirmed in previous studies [2,29]. With respect to the condition in the study, the Rayleigh number[30] Ra equals to 7270 and was less than 10^6, thereby indicating that the flow was laminar in the enclosure [31].

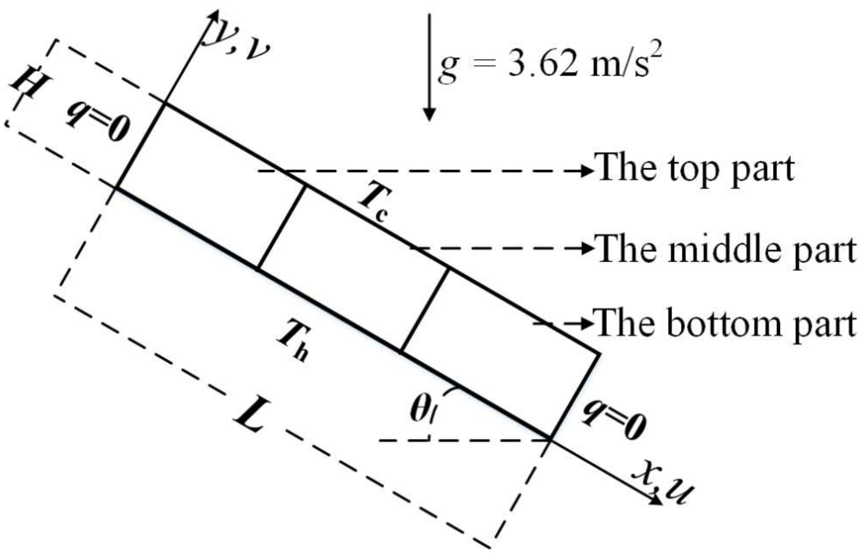

Fig. 1. Schematic model of the CO_2 enclosure

2.2 Mathematical formulation and solution method

The flow state of carbon dioxide in the enclosures was determined based on the Knudsen number ($Kn = \lambda/l$). With respect to the mean free path (λ) of carbon dioxide on Mars surface of approximately 5×10^{-6} m [32] and the characteristic length (l) of the enclosures of 140×10^{-3} m, the Knudsen number of enclosures was 3.6×10^{-6}, and this was significantly lower than 0.001. Therefore, it was considered that fluid flow in the enclosures on Mars surface belonged to continuous flow, and the Navier–Stokes and energy equations were available.

The steady numerical study was solved by the finite volumes method and the fluid was assumed as incompressible. Furthermore, in the study, $\beta \times (T - T_0) \ll 1$, and thus the Boussinesq approximation was applied[33]. The variation in fluid density with temperature was negligible except in buoyancy term[34,35].

The governing equations for the problem were based on the balance between mass, momentum, and energy:

Mass balance:

$$\frac{\partial u}{\partial x}+\frac{\partial \upsilon}{\partial y}=0 \tag{1}$$

Momentum balance:

x-direction:

$$\rho_0\left(u\frac{\partial u}{\partial x}+\upsilon\frac{\partial u}{\partial y}\right)=-\frac{\partial p}{\partial x}+\frac{\partial}{\partial x}\left(\mu\frac{\partial u}{\partial x}\right)+\frac{\partial}{\partial y}\left(\mu\frac{\partial u}{\partial y}\right)+\rho_0 g\beta\left(T-T_0\right)\sin\theta \tag{2}$$

y-direction:

$$\rho_0\left(u\frac{\partial \upsilon}{\partial x}+\upsilon\frac{\partial \upsilon}{\partial y}\right)=-\frac{\partial p}{\partial y}+\frac{\partial}{\partial x}\left(\mu\frac{\partial \upsilon}{\partial x}\right)+\frac{\partial}{\partial y}\left(\mu\frac{\partial \upsilon}{\partial y}\right)-\rho_0 g\beta\left(T-T_0\right)\cos\theta \tag{3}$$

Energy balance:

$$\rho_0\left(u\frac{\partial\left(c_pT\right)}{\partial x}+\upsilon\frac{\partial\left(c_pT\right)}{\partial y}\right)=\frac{\partial}{\partial x}\left(k\frac{\partial T}{\partial x}\right)+\frac{\partial}{\partial y}\left(k\frac{\partial T}{\partial y}\right) \tag{4}$$

Boundary conditions:

$$\left.\begin{array}{ll} T=T_h & \text{at } y=0 \\ T=T_c & \text{at } y=H \\ \dfrac{\partial T}{\partial x}=0 & \text{at } x=0 \text{ and } x=L \end{array}\right\} \tag{5}$$

A feature of the partitions is considered. The partition is sufficiently thin, and thus the temperature difference between the two-sides of partitions is assumed as negligible and the coupled thermal boundary condition is applied to both sides of the partitions.

$$\left.\begin{aligned} T_p^{+} &= T_p^{-} \\ \left(\frac{\partial T}{\partial x}\right)_p^{+} &= \left(\frac{\partial T}{\partial x}\right)_p^{-} \end{aligned}\right\} \quad (6)$$

Commercially available FLUENT 14.0 software, is applied to solve the steady-state numerical solutions. The equations (1)–(4) with corresponding boundary conditions of equation (5) and (6) are achieved via the following solution methods: The pressure-based coupled algorithm is selected as the solution of the governing equation. With respect to the discretization scheme, the least squares cell based method is used for the gradient discretization. The PRESTO! (pressure staggering option) scheme is applied to the pressure interpolation scheme while the second order upwind scheme is applied for energy and momentum equations. The value of residual tolerance $\Delta\tau = 10^{-6}$ is considered as the convergence criterion for the calculation.

The physical property parameters of carbon dioxide used in Fluent are obtained from the National Institute of Standards and Technology (NIST) database. The density of fluid (ρ_0) equals to 0.024 kg/m^3, and thermal expansion coefficient (β) equals to 0.0046 1/K. The dynamic viscosity (μ), thermal conductivity (k) and specific heat of fluid (c_p) are fitted as a function of temperature as follows[36,37] and used in polynomial profile of material properties:

$$\mu(T)_{CO_2} = -2\times10^{-11}T^2 + 6\times10^{-8}T - 1\times10^{-6} \qquad \text{kg/(m}\cdot\text{s)} \quad (7)$$

$$k(T)_{CO_2} = 5\times10^{-8}T^2 + 5\times10^{-5}T - 0.002 \qquad \text{W/(m}\cdot\text{K)} \quad (8)$$

$$c_p(T)_{CO_2} = -1\times10^{-6}T^2 + 0.0017T + 0.4401 \qquad \text{J/(g}\cdot\text{K)} \quad (9)$$

2.3 Grid sensitivity

Grid independence of the solution scheme significantly affects the calculation results of heat transfer and fluid flow. In order to verify the validity of the grid sensitivity, a grid experiment was conducted before the calculations. Uniform mesh sizes in both x and y directions was used in the study owing to the laminar flow in the enclosure. The cases with tilt angle ranging from 0 to 90°, partition numbers of 0, 1, 2, and 3, gravity acceleration of 3.62 m/s^2, and pressure of 1000 Pa were calculated on the grids of three different meshes as follows: Mesh a: grid of 501×71 points; Mesh b: grid of 1001×141 points, and Mesh c: grid of 1501×211 points. A few typical test results of heat flux were shown in Table 1. The definition of average heat flux (q) is given as follows:

$$q = \frac{Q}{L\times d} \quad (10)$$

where Q denotes the heat transfer rate through the enclosure; L denotes the enclosure length; and d denotes the enclosure deep, which equals to 1 m in the study.

Table 1 Grid dependence test model and results

***θ* = 0°**	***θ* = 20°**	***θ* = 90°**

case	N	Mesh	q (W/m²)	case	N	Mesh	q (W/m²)	case	N	Mesh	q (W/m²)
1	0	a	**7.28**	5	0	a	**6.61**	9	0	a	5.02
		b	7.27			b	6.60			b	5.02
		c	7.27			c	6.60			c	5.02
2	1	a	**7.11**	6	1	a	**6.72**	10	1	a	5.72
		b	7.10			b	6.71			b	5.72
		c	7.10			c	6.71			c	5.72
3	2	a	**6.83**	7	2	a	6.20	11	2	a	6.01
		b	6.82			b	6.20			b	6.01
		c	6.82			c	6.20			c	6.01
4	3	a	**6.77**	8	3	a	5.75	12	3	a	6.10
		b	6.76			b	5.75			b	6.10
		c	6.76			c	5.75			c	6.10

The results indicated that the mesh dependence decreased with increases in the tilt angle: (1) When the tilt angle of the enclosure was 0°, for all the cases, the test results of Mesh b and c were the same albeit, lower than Mesh a. (2) When the tilt angle of the enclosure was 20°, for case 5 and case 6, the test results of Mesh b and c were the same albeit lower than that of Mesh a. However, for case 7 and case 8, the test results of Mesh a, b, and c were the same. (3) When the tilt angle of the enclosure was 90°, for all the cases, the test results of Mesh a, b, and c were the same. Hence, Mesh b was applied to Case1 to Case6, and Mesh a was applied to Case7 to Case12, which achieved an optimum compromise between accuracy and computational costs.

Similarly, grid sizes generated in Mesh a, Mesh b, and Mesh c were also selected for other cases with different tilt angles and partition numbers to calculate heat flux through the enclosures, thus obtaining the grid independent results.

3 Model validation

As discussed in the introduction, there is a paucity of investigations on fluid flow and heat transfer inside CO_2 enclosures on Mars surface. The most similar research was conducted by Bhandari et al. [36] who experimentally investigated natural convection in CO_2 filled cylindrical enclosures of a Mars rover to obtain the optimal thickness for the minimum heat transfer through the enclosure. The cylindrical enclosure was filled with carbon dioxide of 1066.6 Pa, and the gravitational acceleration was 9.8 m/s^2. The top and surrounding walls were maintained at 203 K, while the bottom wall was maintained at 243 K. The cylindrical radius was 368.3 mm, and five enclosure thicknesses of 38.1 mm, 50.8 mm, 76.2 mm, 101.6 mm, and 127 mm were considered. The same horizontal cylindrical enclosures as those in [36] were selected for comparison purposes, and the comparison between the results from the paper and those in [36] was shown in Fig. 2. With increasing enclosure thickness, the thermal conductance calculated in the present study agreed well with those in [36].

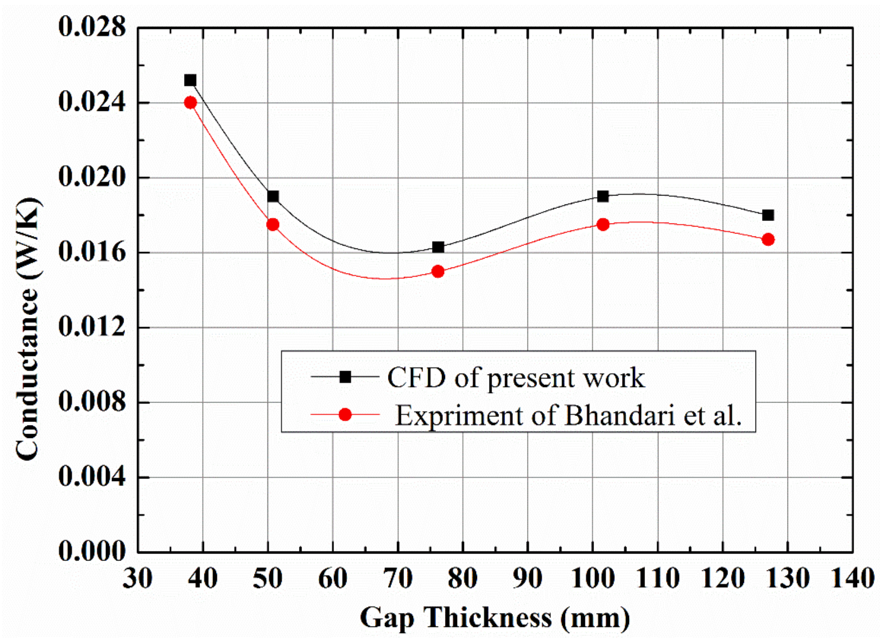

Fig. 2. Comparison of thermal conductance obtained by Bhandari et al. [36] and present study

Additionally, the accuracy of the present numerical procedure was further validated by comparing the present CFD results with the experimental results obtained by Baïri [38] who conducted an experimental investigation of fluid flow and heat transfer in an air cavity on the Earth's surface with two opposite isothermal walls and four adiabatic walls. The tilt angle of the cavity could be varied from 0° to 360° by the rotating framework. The cases with Rayleigh number of 2.64×10^4 and tilt angle of 0°, 45°, 90°, 180°, and 225° were selected for comparison purposes. The results shown in Fig. 3 indicated that a favorable agreement existed between the results in this paper and those in [38]. Therefore, it was evident that the CFD calculation model and method could be reliably applied in the present study.

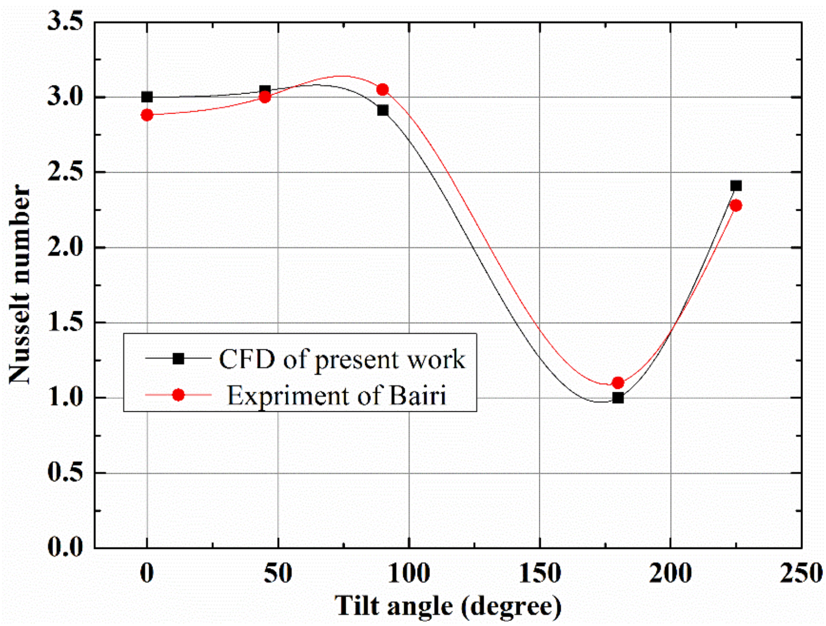

Fig. 3. Comparison of the Nusselt numbers obtained by Baïri [38] with those in the present study

4 Results and discussion

4.1 Velocity and thermal distributions

The analysis in the study indicated that the velocity and thermal distributions were related to the tilt angle and partition number. Thus, a parameter was fixed to investigate the influence of the other parameter on fluid flow and heat transfer in the enclosure.

4.1.1 Influence of tilt angle

Fig. **4** showed the evolution of velocity contours, streamlines, and isotherms for the enclosure with two partitions when the tilt angle increased. The streamlines in Fig. 4a showed the flow direction of convections. When the enclosure sloped, three different flow regimes successively occurred in the enclosure, and there were two critical angles corresponding to the two turning points between the three flow regimes. As shown in Fig. 4, the flow appeared as a Rayleigh–Bénard convection at θ = 0°. Rayleigh–Bénard convection is a type of multiple-cell convection, and this is also observed in a few other studies[39,40]. When the θ increased to θ_{cri1} = 12.9°, the pattern changed into a transition convection, and subsequently when the θ increased to θ_{cri2} = 24.6°, the flow mode changed to a single-cell convection and persisted until θ = 90°. Thus, the complete mode changing process was divided into three regimes. The first, second, and third regimes corresponded to the Rayleigh–Bénard convection, transition convection, and single-cell convection, respectively. The analysis of our results indicated that the velocity fields, thermal distributions, and heat transfer were closely correlated to the different regimes.

In the first regime, the flow in all parts of the enclosure were Rayleigh–Bénard convection. At this condition, as shown in Fig. 4b(1), the isotherm contour was a type of four-Ω structure. With increasing tilt angle, the structure gradually transformed to a three-and-a-half Ω form although the isotherms density near the hot and cold walls were almost maintained as unchanged as shown in Fig. 4b(2).

When the enclosure was titled sequentially, the buoyant shear flow along the hot wall increased, thereby leading to an increase in the flow strength in x-direction and a decrease in the flow strength in y-direction in all parts of the enclosure. Thus, the Rayleigh–Bénard convections began to gradually revert to unicellular ones from θ_{cri1} = 12.9º to θ_{cri2} = 24.6º. The flow mode continuously evolved during the regime until the multiple-cell pattern completely faded at the inclination of θ_{cri2}. During the second regime, as the example of θ = 15° shown in Fig. 4b(3) and Fig. 4a(3), the isotherm structure changed to a two-and-a-half-Ω form, and the profiles in the top part was distorted and associated with the single-cell convection. Additionally, when the angle increased, the heated stream was pushed farther away from the cold wall, and thus the isotherms density near the cold wall decreased. It implied that the temperature gradient of the stream close to the cold wall was lower than that of multiple-cell Rayleigh–Bénard pattern. Similarly, the temperature gradient of the stream near the hot wall also exhibited the same tendency. Hence, the lower temperature gradient resulted in decreased heat transfer, and this was confirmed by verifying the heat flux as discussed in section 4.2.1.

When the tilt angle extended beyond θ_{cri2}, the velocity in x-direction significantly exceeded that in y-direction owing to the stronger buoyancy force along the hot wall. Hence, as shown in Fig. 4a(4), Fig. 4a(5), and Fig. 4a(6), the steady single-cell convection was promptly established in all parts. The flow circulating clockwise was caused by the position of the hot and cold surfaces while the core of the region was relatively stagnant, and this was also confirmed by Ganguli et al. [6]. In the regime, the velocity of the flow increased with increasing tilt angle when the flow mode persisted as single-cell, and this resulted in a strengthening of the flow field. Simultaneously, as shown in Fig. 4b(4), Fig. 4b(5), and Fig. 4b(6), the isotherms transformed to a skew-symmetric distortion (hot fluid upwards in the side of the hot plate and cold fluid downwards in the side of the cold plate) in all parts of the enclosure with dense isotherms near the longitudinal walls.

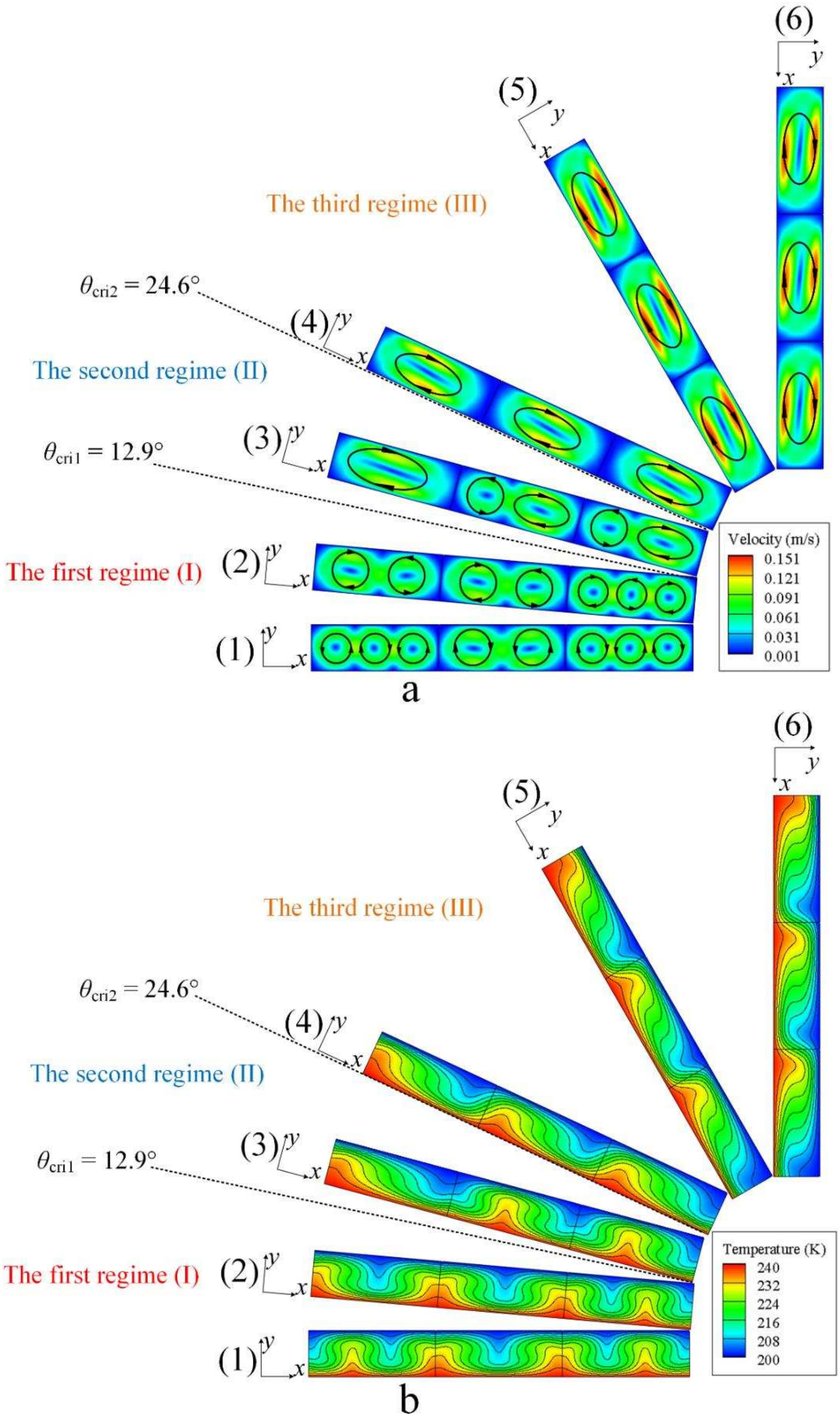

Fig. 4. Velocity and temperature contours in enclosures at L = 1000 mm, H = 140 mm, ΔT = 40 K，N = 2: (1) θ = 0°; (2) θ = 5°; (3) θ = 15°; (4) θ = 25°; (5) θ = 60°; (6) θ = 90°

4.1.2 Influence of partition number

In this section, the effect of the partition number (N = 0, 1, 2 and 3) on natural convection heat transfer was discussed. The different critical values of the tilt angle for the enclosures with different partition numbers are listed in Table 2 (the maximum error was 0.1°). It should be noted that the transition from Rayleigh–Bénard convection to single-cell convection could be brought forward to a lower tilt angle when the partition number increased. This was interpreted that the more parts formed in the enclosure, the less room the flow could move, and this reduced the probability of the single cells splitting into the multiple ones. In this case, less contribution of the buoyancy force was devoted to the splitting process (y-direction). Therefore, the buoyancy force in the x-direction was boosted, and this make single-cell convection occur more easily in the enclosure. In summary, the presence of the partition played a role in advancing the formation of single-cell convection.

Table 2 Values of the critical angle for the enclosures with different partition numbers

N	**θ_{cri1} (degree)**	**θ_{cri2} (degree)**
0	18.9	33.3
1	13.6	28.6
2	12.9	24.6
3	2	16.6

The influence of the partitions on the three different regimes was shown in Fig. 5, Fig. 6, and Fig. 7. The streamline and isotherm fields were shown for tilt angles of 0°, 20°, and 90° corresponding to the first, second, and third regimes, respectively.

In the first regime, there was no significant variation in the flow pattern when the number of the partition increased. As shown in Fig. 5, the velocity field in each enclosure with different partition number was the eight-cell Rayleigh–Bénard corresponding to the same temperature distribution of the four-Ω structure. This was because the flow pattern in the condition was mainly determined by the stream circulation caused by the buoyancy force along the y-direction, however, the influence of the partition on the flow strength in y-direction was negligible.

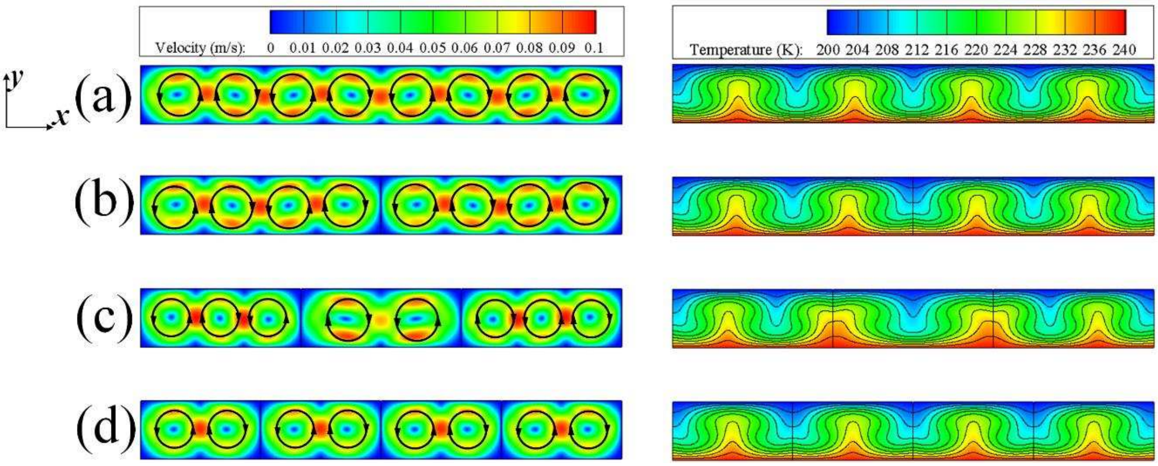

Fig. 5. Velocity and temperature contours in enclosures at L = 1000 mm, H = 140 mm, ΔT = 40 K, θ = 0°:

(a) N = 0; (b) N = 1; (c) N = 2; (d) N = 3

The effect of the partition was the most significant in the second regime when compared with that in other two regimes. This was because the flow was unstable in the transition convection, namely, both the flow pattern and isotherm contour were easy to destroy. As shown in Fig. 6, for N = 0, the flow pattern was the two-small-cell-between-three-big-cell form. The isotherm contour was the two-and-a-half-Ω structure. With respect to N = 1, the flow mode changed to two one-small-between-two-big-cell patterns, and the isotherm contours of three-and-a-half-Ω developed at the moment. With respect to N = 2, the flow appeared as one single-cell in the middle part and two one-big-and-one-small cells in the side parts. For isotherm contours, the Ω structure was transformed to two-and-a-half form again, but an evident deformation in the isotherms was observed. With respect to N = 3, the flow mode was completely altered to the mode of the third regime. At this moment, both the character of the velocity and temperature fields in each part conformed to the single-cell mode. In summary, with increasing partitions introduced into the enclosure, both the flow pattern and isotherm contour got closer to those of the third regime.

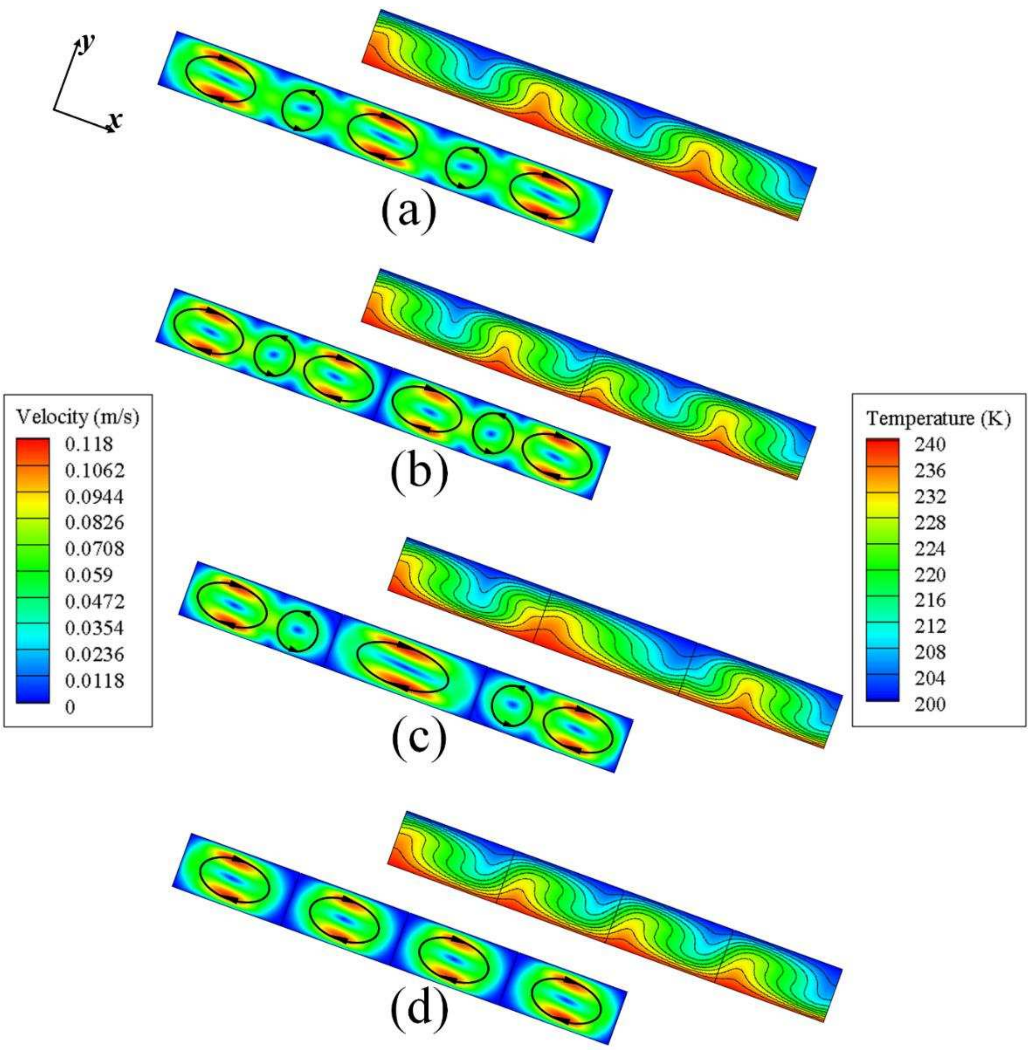

Fig. 6. Velocity and temperature contours in enclosures at L = 1000 mm, H = 140 mm, ΔT = 40 K, θ = 20°: (a) N = 0; (b) N = 1; (c) N = 2; (d) N = 3

In the third regime, with the function of the partitions, the big single cell was divided into several small single cells, which was equivalent to the multiple-cell convection. As shown in Fig. 7, the streamlines and isotherm contours in different parts of an enclosure were approximately identical, and only a single cell was indicated in each part. Additionally, it should be noted that the partition hindered the fluid flow in x-direction, and this implied that the more parts formed in the enclosure, the lower velocity of the fluid in x-direction was. However, as previously discussed, the influence of the partition on the flow strength in y-direction was limited. Hence, the isotherm contours in different enclosures became increasingly contorted with an increase number of partitions.

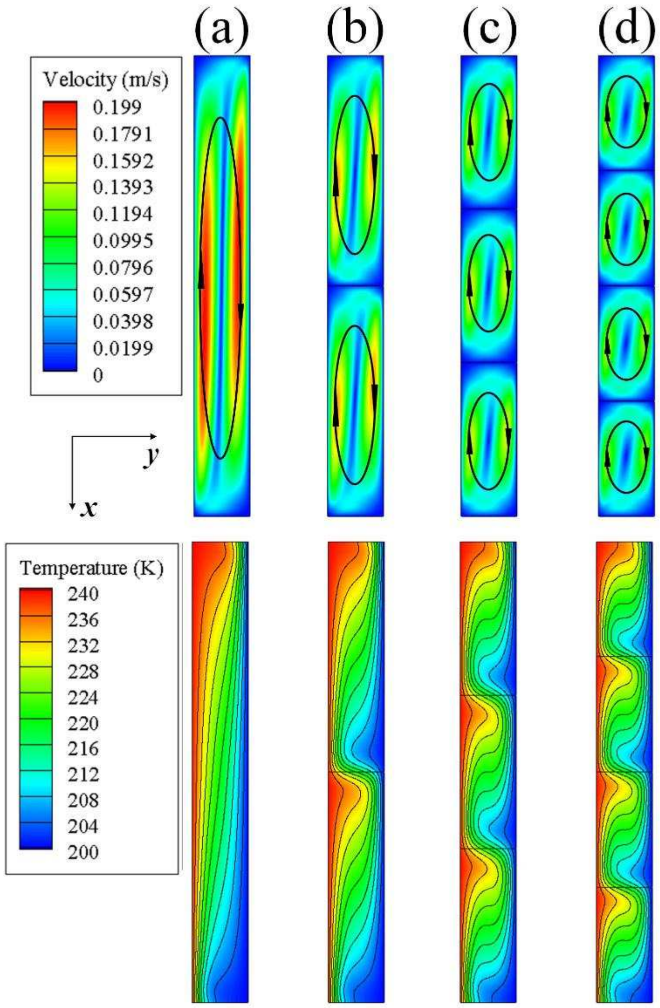

Fig. 7. Velocity and temperature contours in enclosures at L = 1000 mm, H = 140 mm, ΔT = 40 K, θ = 90°: (a) N = 0; (b) N = 1; (c) N = 2; (d) N = 3

4.2 Convection heat flux through the enclosure

4.2.1 Combined influence of tilt angle and partition number

In this section, the combined influence of two parameters (N, θ) on the heat flux through an enclosure was examined. Figure 8 showed the heat flux as a function of the enclosure tilt angle and the partitions number.

In the first regime, the effect of tilt angle on the heat flux was not evident because the temperature gradient near the walls was maintained as almost unchanged with increasing inclination angle as shown in

Fig. 4b(1) and Fig. 4b(2). The highest value of the heat flux corresponded to the original enclosure without partitions. The introduction of the three partitions reduced the heat flux by 10.6%. This was because increased partitions attached to the enclosure suppressed the velocity of fluid flow, although the flow pattern remained almost unchanged as shown in Fig. 5.

With respect to a higher tilt angle, over the θ_{cri1}, convection flow changed into the transition regime. As θ further increased, the heat flux decreased sharply. During the beginning and the end stages of the regime, with a certain increase in the tilt angle, there was a significant decrease on the q-θ-curve, and this was caused by the changes in the flow mode as discussed in 4.1.1. However, the decrease in the heat flux through the enclosure with partitions was lower than that of non-partitioned enclosure. As shown in Fig. 8, the heat flux completely decreased by 38.0% in the empty enclosure, while the transition process in the enclosure with three partitions just caused a 14.2% decrease in the overall heat flux. In other words, the raising partition number suppressed the reduction in the heat flux. Additionally, significant changes in the heat flux occurring at different tilt angles also suggested that the transition with the ever-changing θ was brought forward when the partition number increased.

When the inclination passed the θ_{cri2}, the single-cell convection immediately contributed, and the heat flux tended to increase when the tilt angle increased from θ_{cri2} to a certain degree (θ = 80°, 75°, 70°, 60° for N = 0, 1, 2, 3) and then decreased slowly till θ = 90°. However, the discrepancy between the heat fluxes of the four curves decreased with increasing tilt angle. This was because when the tilt angle increased, the difference in the isotherm contour near the hot and cold walls between the enclosures with different number of partitions became less evident. Additionally, in the third regime, the highest value of the heat flux referred to the enclosure with three partitions, and this was reversed to the lowest value in the first regime. This was validated by isotherms close to the longitudinal walls as shown in Fig. 7 where the isotherms were sparsest at N = 0, thereby demonstrating a poorer heat transfer in the enclosure. When N increased, the isotherm density in the neighborhood of the longitudinal walls increased, indicating an enhancement in overall heat transfer through the enclosure. This explained the augmentation in the heat flux with increasing partition number. Nevertheless, the discrepancy between the heat fluxes of the four curves decreased with an increase in the partition number. This was because that the more partitions were attached to the wall, the less variation of the isotherms would appear as shown in Fig. 7. In summary, the influence of the partition number on heat flux became less evident when the partition number or the tilt angle increased.

It should also be noted that when the partitions were attached to the isothermal surface, for various tilt angles, the maximum heat flux through the enclosure decreased, while the minimum heat flux increased as shown in Table 3. The results indicated that the influence of the tilt angle on the heat flux through the partitioned enclosures was less significant than that in the non-partitioned enclosure because the partitions exhibited a relaxative impact on the variation in heat flux. Therefore, the partitions played a crucial role in alleviating the fluctuation of heat transfer with changes in the tilt angle as faced by a Mars Rover operating on rugged Mars surface.

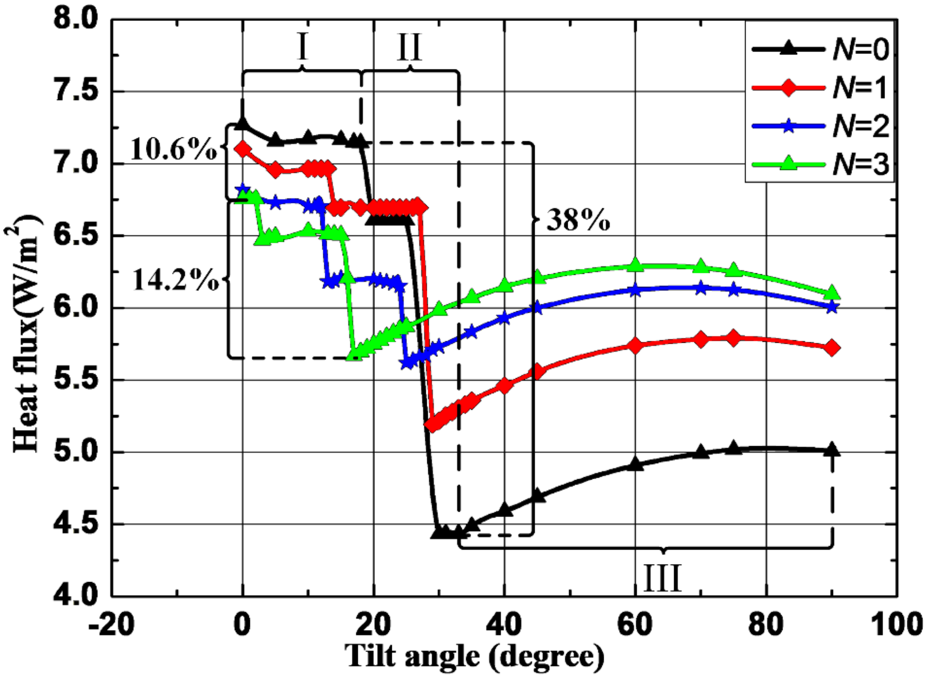

Fig. 8. Heat flux as a function of tilt angle for different partition numbers (I, II, and III refer to the first, second, and third regimes, respectively, in the non-partitioned enclosure as an example)

Table 3 Values of the minimum and maximum heat flux through the enclosures for different partition numbers with changes in the tilt angle

N	q_{min} (W/m^2)	q_{max} (W/m^2)
0	4.43	7.27
1	5.19	7.10
2	5.62	6.82
3	5.67	6.76

4.2.2 Opposite effect of partitions on the first and third regime

Based on the concept of field synergy principle [41], the synergy angle, namely the intersection angle between the velocity vector of fluid flow and the temperature gradient vector, can reflect the amount of heat transfer. When the synergy angle (θ_{syn}) approaches 0° and 180°, heat transfer is strengthened. It is physically shown that when velocity vector of fluid flow and temperature gradient vector are parallel to each other, the contribution of fluid to the heat transfer reaches the maximum. Conversely, when velocity vector is perpendicular to temperature gradient vector, heat transfer cannot be enhanced by fluid flow. The synergy angle is defined as follows:

$$\theta_{syn} = \arccos\left(\frac{\vec{V} \times \vec{\nabla T}}{|\vec{V}| \times |\vec{\nabla T}|}\right) \quad (11)$$

where $\vec{V}$ denotes the velocity vector and $\vec{\nabla T}$ denotes the temperature gradient vector.

In order to illustrate the opposite effects of partitions on the heat transfer between the first and the third regime, the synergy angle fields for enclosures with different partition numbers are shown in Fig. 9 and Fig. 10. The enclosures at the angles of 0° and 90° were selected to denote the first (Fig. 9) and third regimes (Fig. 10), respectively, in this section.

In the first regime, the original flow pattern had already been multiple-cell convection in the non-partitioned enclosure. When the partitions were placed in the enclosure, they only slightly impacted the synergy angle fields as shown in Fig. 9. Thus, synergy angle fields were extremely similar in the enclosures with different partition numbers in the first regime. However, as shown in Fig. 8, the heat flux slightly decreased with increasing partition number, and this was mainly caused by the decrease in fluid velocity due to the impact of the partitions as shown in Fig. 5.

With respect to the third regime, synergy angle field significantly changed when the partitions were attached to the enclosure as shown in Fig. 10. As discussed in 4.1.2, the big single cell was divided into small single cells by the partitions, and the flow structure in the complete enclosure was equivalent to multiple-cell convection. In this case, the stream along the hot wall was deflected parallel to the y-axis by the partitions at the relative positions corresponding to x/L = 1/2 for N = 1; x/L = 1/3 and x/L = 2/3 for N = 2; x/L = 1/4, x/L = 2/4, and x/L = 3/4 for N = 3. Therefore, the velocity vector of the flow near the partitions was paralleled to the temperature gradient vector, and heat transfer was thus enhanced. As shown in Fig. 10, the more partitions in the enclosure, the more regions in which the synergy angle was closer to 0° and 180°, and this lead to higher heat transfer through the enclosure as shown in Fig. 8.

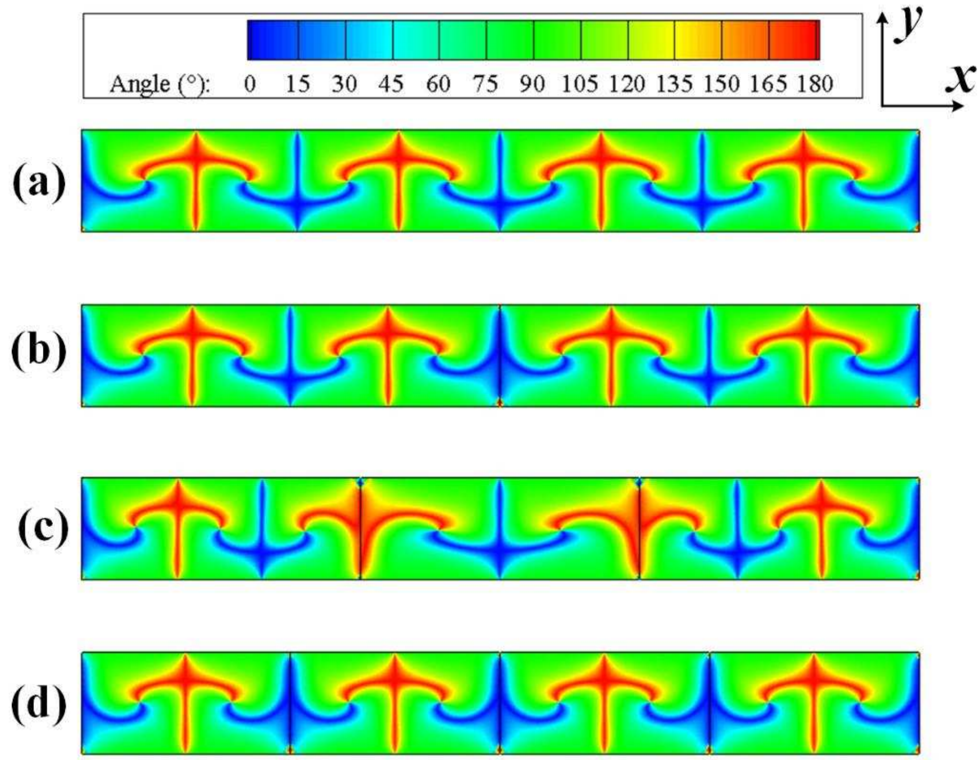

Fig. 9. Synergy angle fields of horizontal enclosures (the first regime) at L = 1000 mm, H = 140 mm, ΔT = 40 K: (a) N = 0; (b) N = 1; (c) N = 2; (d) N = 3

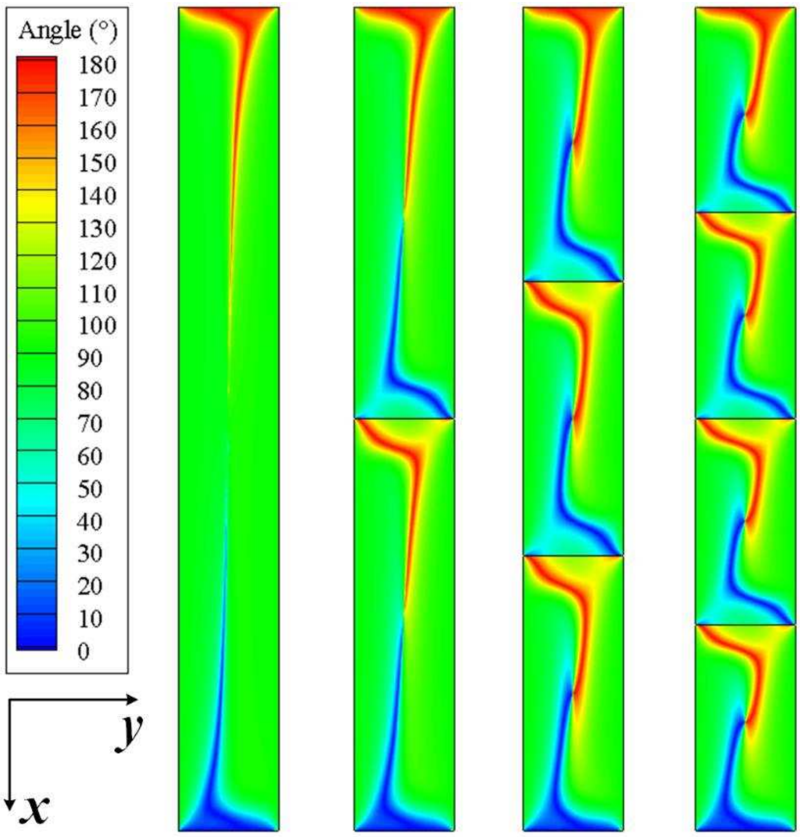

Fig. 10. Synergy angle fields of vertical enclosures (the third regime) at L = 1000 mm, H = 140 mm, ΔT = 40 K: (a) N = 0; (b) N = 1; (c) N = 2; (d) N = 3

5 Conclusions

In the study, fluid flow and heat transfer in inclined and fully divided CO_2 enclosures with partitions on Mars surface were numerically investigated. The ranges of parameter in the study were p = 1000 Pa, g = 3.62 m/s^2, ΔT = 40 K, AR = 7.14, Ra = 7270, N = 0, 1, 2, and 3, and $0° \le \theta \le 90°$. The primary conclusions were summarized as follows:

1) With increasing tilt angle, three different flow regimes successively occurred in the enclosure as follows: the Rayleigh–Bénard convection, transition convection, and single-cell convection.

2) Two critical angles existed and corresponded to the two turning points between the three flow regimes: θ_{cri1} = 18.9° and θ_{cri2} = 33.3° for the non-partitioned enclosure; θ_{cri1} = 13.6° and θ_{cri2} = 28.6° for the enclosure with a partition; θ_{cri1} = 12.9° and θ_{cri2} = 24.6° for enclosure with two partitions; θ_{cri1} = 2° and θ_{cri2} = 16.6° for the enclosure with three partitions.

3) The transition from Rayleigh–Bénard convections to single-cell convection could be brought forward to a lower tilt angle by increased partition number. The transition regime was the most unstable regime, and both the flow pattern and isotherm contour would be closer to those of the third regime when the partition was attached to the enclosure.

4) During the beginning and the end stage of the second regime, there were two significant decreases in the heat flux, and the rate of the overall decrease in the heat flux reduced with increasing partition number as follows: 38.0% for the non-partitioned enclosure and 14.2% for the enclosure with three partitions. In the third regime, the influence of the partition number on heat flux became less evident when the partition

number or the tilt angle increased.

5) The partitions moderated the fluctuation in heat flux through the enclosure for various tilt angles. When the tilt angle changed, the heat flux fluctuated from 4.43 W/m^2 to 7.27 W/m^2 for the non-partitioned enclosure and from 5.67 W/m^2 to 6.76 W/m^2 for the enclosure with three partitions. The maximum heat flux through the enclosure decreased, while the minimum heat flux increased.

Declarations of interest

The authors declare that there is no conflict of interest.

Acknowledgement

The study was supported by the EU Marie Curie Actions-International Incoming Fellowships (FP7-PEOPLE-2013-IIF-913576).

References

[1] L. Xiyun, Z. Lixian, Numerical study of natural convection flow in a vertical slot, Acta Mech. Sin. 15 (1999) 215–224. doi:10.1007/BF02486149.

[2] H. Manz, Numerical simulation of heat transfer by natural convection in cavities of facade elements, Energy Build. 35 (2003) 305–311. doi:10.1016/S0378-7788(02)00088-9.

[3] F. Ampofo, T.G. Karayiannis, Experimental benchmark data for turbulent natural convection in an air filled square cavity, Int. J. Heat Mass Transf. 46 (2003) 3551–3572. doi:10.1016/S0017-9310(03)00147-9.

[4] Y. Zhou, R. Zhang, I. Staroselsky, H. Chen, Numerical simulation of laminar and turbulent buoyancy-driven flows using a lattice Boltzmann based algorithm, Int. J. Heat Mass Transf. 47 (2004) 4869–4879. doi:10.1016/j.ijheatmasstransfer.2004.05.020.

[5] W. Wu, C.Y. Ching, A.A. Ganguli, A.B. Pandit, J.B. Joshi, Y. Zhou, R. Zhang, I. Staroselsky, H. Chen, H. Manz, F. Ampofo, T.G. Karayiannis, L. Xiyun, Z. Lixian, S.H. Yin, T.Y. Wung, K. Chen, A. Bejan, C.L. Tien, Natural convection in an air layer enclosed within rectangular cavities, Int. J. Heat Mass Transf. 87 (2009) 711–727. doi:10.1016/j.cherd.2008.11.005.

[6] A.A. Ganguli, A.B. Pandit, J.B. Joshi, CFD simulation of heat transfer in a two-dimensional vertical enclosure, Chem. Eng. Res. Des. 87 (2009) 711–727. doi:10.1016/j.cherd.2008.11.005.

[7] I. V. Miroshnichenko, M.A. Sheremet, Turbulent natural convection heat transfer in rectangular enclosures using experimental and numerical approaches: A review, Renew. Sustain. Energy Rev. 82 (2018) 40–59. doi:10.1016/j.rser.2017.09.005.

[8] C.Y. Soong, P.Y. Tzeng, D.C. Chiang, T.S. Sheu, Numerical study on mode-transition of natural convection in differentially heated inclined enclosures, Int. J. Heat Mass Transf. 39 (1996) 2869–2882. doi:10.1016/0017-9310(95)00378-9.

[9] P.Y. Tzeng, C.Y. Soong, T.S. Sheu, Numerical investigation of transient flow-mode transition of laminar natural convection in an inclined enclosure, Numer. Heat Transf. Part A Appl. 31 (1997) 193–206. doi:10.1080/10407789708914032.

[10] I. Girgis, Numerical and experimental investigations of natural convection in inclined air enclosures, 38th Aerosp. Sci. Meet. Exhib. (2000). doi:10.2514/6.2000-995.

[11] I. V. Miroshnichenko, M.A. Sheremet, Turbulent natural convection combined with thermal surface

radiation inside an inclined cavity having local heater, Int. J. Therm. Sci. 124 (2018) 122–130. doi:10.1016/j.ijthermalsci.2017.09.023.

[12] R. Jetli, S. Acharya, E. Zimmerman, Influence of baffle location on natural convection in a partially divided enclosure, Numer. Heat Transf. 10 (1986) 521–536. doi:10.1080/10407788608913532.

[13] K.M. Kelkar, S. V. Patankar, Numerical prediction of natural convection in square partitioned enclosures, Numer. Heat Transf. Part A Appl. 17 (1990) 269–285. doi:10.1080/10407789008944743.

[14] Y.S. Sun, A.F. Emery, Multigrid computation of natural convection in enclosures with a conductive baffle, Numer. Heat Transf. Part A Appl. 25 (1994) 575–592. doi:10.1080/10407789408955967.

[15] C.D. Sankhavara, H.J. Shukla, Natural Convection in a Partially Divided Rectangular Enclosure, (2006) 1–14. doi:10.2514/6.2006-3593.

[16] G.G. Ilis, M. Mobedi, H.F. Öztop, Heat transfer reduction due to a ceiling-mounted barrier in an enclosure with natural convection, Heat Transf. Eng. 32 (2011) 429–438. doi:10.1080/01457632.2010.483889.

[17] N. Yucel, A.H. Ozdem, Natural convection in partially divided square enclosures, Heat Mass Transf. Und Stoffuebertragung. 40 (2003) 167–175. doi:10.1007/s00231-002-0361-4.

[18] G. Nardini, M. Paroncini, R. Vitali, An Experimental and Numerical Analysis of Natural Convective Heat Transfer in a Square Cavity With Five Discrete Heat Sources, J. Heat Transfer. 138 (2016) 122502. doi:10.1115/1.4034160.

[19] Y. Bae, S.H. Kim, J.K. Seo, Y.I. Kim, Analytical Modeling of Natural Convection in a Tall Rectangular Enclosure with Multiple Disconnected Partitions, Nucl. Eng. Technol. 48 (2016) 925–931. doi:10.1016/j.net.2016.02.021.

[20] A. Bejan, Natural convection heat transfer in a porous layer with internal flow obstructions, Int. J. Heat Mass Transf. 26 (1983) 815–822. doi:10.1016/S0017-9310(83)80105-7.

[21] H. Turkoglu, N. Yücel, Natural convection heat transfer in enclosures with conducting multiple partitions and side walls, Heat Mass Transf. 32 (1996) 1–8. doi:10.1007/s002310050084.

[22] K. Kahveci, A differential quadrature solution of natural convection in an enclosure with a finite-thickness partition, Numer. Heat Transf. Part A Appl. 51 (2007) 979–1002. doi:10.1080/10407790601184371.

[23] N. Williamson, S.W. Armfield, The stability of conjugate natural convection boundary layers, Anziam J.electron.suppl. 52 (2010) 5–8. doi:10.21914/anziamj.v52i0.3886.

[24] M. Khatamifar, W. Lin, S.W. Armfield, D. Holmes, M.P. Kirkpatrick, Conjugate natural convection heat transfer in a partitioned differentially-heated square cavity, Int. Commun. Heat Mass Transf. 81 (2017) 92–103. doi:10.1016/j.icheatmasstransfer.2016.12.003.

[25] S. Acharya, C.H. Tsang, Natural Convection in a Fully Partitioned, Inclined Enclosure, Numer. Heat Transf. 8 (1985) 407–428. doi:10.1080/01495728508961863.

[26] C.H. Tsang, S. Acharya, Natural convection in an inclined enclosure with an off-center complete partition, Heat Mass Transf. 9 (1986) 217–239. doi:10.1080/10407788608913474.

[27] M. Mamou, M. Hasnaoui, P. Vasseur, E. Bilgen, Natural Convection Heat Transfer in Inclined Enclosures With Multiple Conducting Solid Partitions, Numer. Heat Transf. Part A Appl. 25 (1994) 295–315. doi:10.1080/10407789408955950.

[28] Y. Sun, G. Lin, X. Bu, L. Bai, C. Xiao, D. Wen, A numerical study of fluid flow and heat transfer in carbon dioxide enclosures on mars, Energies. 11 (2018) 1–19. doi:10.3390/en11040756.

[29] W. Wu, C.Y. Ching, The effect of the top wall temperature on the laminar natural convection in rectangular cavities With different aspect ratios, J. Heat Transfer. 131 (2009) 1–11.

doi:10.1115/1.2993138.

[30] S.Z. Heris, M.B. Pour, O. Mahian, S. Wongwises, A comparative experimental study on the natural convection heat transfer of different metal oxide nanopowders suspended in turbine oil inside an inclined cavity, Int. J. Heat Mass Transf. 73 (2014) 231–238. doi:10.1016/j.ijheatmasstransfer.2014.01.071.

[31] N.C. Markatos, K.A. Pericleous, (1984) Laminar and turbulent natural convection in an enclosed cavity, Int. J. Heat Mass Transf. (1983) 755–772. http://www.sciencedirect.com/science/article/pii/0017931084901455.

[32] R.B. Noll, M.B. Mcelroy, R. Noll, Engineering Model of the Mars Atmosphere, AIAA 13th Aerosp. Sci. Meet. (1975) 75–197. doi:10.2514/6.1975-197.

[33] ANSYS Inc, Fluent 14.0 Theory Guide, 2013.

[34] C.J. Ho, D.S. Chen, W.M. Yan, O. Mahian, Buoyancy-driven flow of nanofluids in a cavity considering the Ludwig-Soret effect and sedimentation: Numerical study and experimental validation, Int. J. Heat Mass Transf. 77 (2014) 684–694. doi:10.1016/j.ijheatmasstransfer.2014.05.059.

[35] O. Mahian, A. Kianifar, S.Z. Heris, S. Wongwises, Natural convection of silica nanofluids in square and triangular enclosures: Theoretical and experimental study, Int. J. Heat Mass Transf. 99 (2016) 792–804. doi:10.1016/j.ijheatmasstransfer.2016.03.045.

[36] P. Bhandari, P. Karlmann, K. Anderson, K. Novak, T.N. Aeronautics, P.T. Engineer, S. Thermal, E. Group, T. Engineer, T. Hardware, F. Systems, S.T. Engineer, CO-2 Insulation for Thermal Control of the Mars Science Laboratory, 41st Int. Conf. Environ. Syst. (2011) 1–16. doi:10.2514/6.2011-5119.

[37] P. Bhandari, K.R. Anderson, CFD Analysis For Assessing The Effect Of Wind On The Thermal Control Of The Mars Science Laboratory Curiosity Rover, 43rd Int. Conf. Environ. Syst. (2013) 1–14. doi:10.2514/6.2013-3325.

[38] A. Baïri, Nusselt-Rayleigh correlations for design of industrial elements: Experimental and numerical investigation of natural convection in tilted square air filled enclosures, Energy Convers. Manag. 49 (2008) 771–782. doi:10.1016/j.enconman.2007.07.030.

[39] C.J. Ho, D.S. Chen, W.M. Yan, O. Mahian, Rayleigh-Bénard convection of Al2O3/water nanofluids in a cavity considering sedimentation, thermophoresis, and Brownian motion, Int. Commun. Heat Mass Transf. 57 (2014) 22–26. doi:10.1016/j.icheatmasstransfer.2014.07.014.

[40] H.F. Öztop, P. Estellé, W.M. Yan, K. Al-Salem, J. Orfi, O. Mahian, A brief review of natural convection in enclosures under localized heating with and without nanofluids, Int. Commun. Heat Mass Transf. 60 (2015) 37–44. doi:10.1016/j.icheatmasstransfer.2014.11.001.

[41] Z.Y. Guo, W.Q. Tao, R.K. Shah, The field synergy (coordination) principle and its applications in enhancing single phase convective heat transfer, Int. J. Heat Mass Transf. 48 (2005) 1797–1807. doi:10.1016/j.ijheatmasstransfer.2004.11.007.

Nomenclature

AR	enclosure aspect ratio	Greek symbols	
c_p	specific heat capacity (J/g·K)	β	thermal expansion coefficient (1/K)
d	enclosure deep (mm or m)	λ	mean free path (m)
g	gravitational acceleration (m/s^2)	μ	dynamic viscosity (kg/m·s)
H	thickness of enclosure (mm)	ρ	density of fluid (kg/m^3)
Kn	Knudsen number	ρ_0	constant density of the flow (kg/m^3)

k	thermal conductivity (W/m·K)	ΔT	difference in temperatures $\Delta T = T_h - T_c$ (K)
L	length of the layer (mm or m)	$\Delta\tau$	residual tolerance
l	characteristic length (m)	θ	tilt angle (degree)
N	partition number	θ_{crit1}	critical angle between the first and second regimes (degree)
p	pressure (Pa)		
Q	Heat transfer rate(W)	θ_{crit2}	critical angle between the second and third regimes (degree)
q	heat flux (W/m^2)		
Ra	Rayleigh number	θ_{syn}	synergy angle (degree)
T	temperature (K)		
T_0	operating temperature (K)	Subscripts	
u	velocity components in x direction (m/s)	c	cold
$\vec{V}$	velocity vector	h	hot
$\overrightarrow{\nabla T}$	temperature gradient vector	max	maximum
v	velocity components in y direction (m/s)	min	minimum
x	x coordinate location (mm)	p	partition
y	y coordinate location (mm)		